Journal of Hazardous Materials, Volume 388, April 2020, Article number 122037
DOI:10.1016/j.jhazmat.2020.122037

Remediation of cadmium and lead polluted soil using thiol-modified biochar

Jiajun Fan[a,b], Chao Cai[a], Haifeng Chi[a], Brian J. Reid[a,c], Frédéric Coulon[d], Youchi Zhang[a,*], Yanwei Hou[a,b,*]

[a] Key Lab of Urban Environment and Health, Institute of Urban Environment, Chinese Academy of Sciences, Xiamen 361021, China

[b] College of Chemical Engineering, Huaqiao University, Xiamen 361021, China

[c] School of Environmental Sciences, University of East Anglia, Norwich NR47TJ, UK

[d] School of Water, Energy and Environment, Cranfield University, Cranfield MK43 0AL, UK

[*] Corresponding authors.

E-mail addresses: yczhang@iue.ac.cn (Y. Zhang), houyw@hqu.edu.cn (Y. Hou).

Abstract

Thiol-modified rice straw biochar (RS) was prepared by an esterification reaction with β-mercaptoethanol and used for the remediation of Cd and Pb polluted soils. Modified biochar was characterized through elemental analysis, BET analysis, FE-SEM, FT-IR and XPS. These analyticalcharacterizations confirmed that the thiol groups were successfully grafted onto the surface of the biochar and were involved in the metal ion complexation. The batch sorption experiments showed that Cd^{2+} and Pb^{2+} sorption onto RS followed a pseudo second order kinetic model and a Langmuir isotherm. The maximum adsorption capacities for Cd^{2+} and Pb^{2+}were 45.1 and 61.4 mg g^{-1}, respectively in the single-metal systems. In contrast, Cd^{2+} was selectively adsorbed over Pb^{2+} by RS in the binary-metal systems. Both Cd^{2+} and Pb^{2+} were mainly removed through surface complexation. The soil incubation experiments further showed that RS reduced the available Cd concentrations up to 40% while available Pb concentrations was reduced up to 11%. Overall, this study demonstrates thiol-modified biochar can effectively enhance the remediation of heavy metal polluted soils.

Keywords: Thiol-modification, Rice straw biochar, Heavy metal pollution, Surface complexation, Soil remediation.

1 Introduction

Cd and Pb contamination of soil throughout the world has become a priority environmental concern [1, 2]. As typical heavy metals, Cd and Pb are identified as priority pollutants by the US Environmental Protection Agency. Anthropogenic activities such as mining, smelting, chemical production and factory emissions dispose large amounts of Cd and Pb into soil, and cause widespread soil contamination[3, 4]. A recent soil survey in China reported approximately 19% of farmland soils to be polluted, and Cd and Pb were identified as the two main pollutants[5]. Shi et al. (2019) reported that Cd concentrations in soils in China gradually increase between 1981 and 2016 due to mining activities, sewage irrigation, and fertilizer application into agricultural soils[6].

Considerable research effort has been devoted to developing methods for the remediation of heavy metal contaminated soils. Soil remediation technologies currently being used include chemical immobilisation[7,8], chemical washing[9], physical technologies[10], phytoremediation[11, 12] and microbial remediation[13, 14]. Although different efficiency, costs and drawbacks have been reported for these technologies, chemical immobilisation has been reported to be a superior choice due to its simplicity, low cost and high efficiency[15]. Chemical immobilisation can decrease mobility and bioavailability of heavy metals through a series of reactions, including ion exchange, adsorption, complexation and precipitation, by adding either organic or inorganic amendments into soil[16-18]. To date, a wide range of novel materials have

been proposed as immobilization agents, including biochar materials, phosphates-containing materials and Si-rich minerals[19-21].

Biochar is a carbon-rich material produced by pyrolysis of organic matter, such as agricultural bio-waste, under an oxygen-limited environment[22]. Biochars have been reported to immobilize heavy metals in soil[22, 23]. However, practical applications at field scale have not consistently shown high levels of success[24, 25]. Thus, there is a need to optimize biochar materials to obtain better remediation outcomes. To date, a number of modification methods have been developed, including acid/base treatment[26, 27], loading with minerals[28, 29] and/or nano-particles[30, 31], and addition of organic functional groups[32-34]. Further to this, surface modification by grafting thiol functional groups, has been proposed as a potentially effective strategy; as thiol groups have a high affinity for heavy metal ions such as Hg^{2+}, Cu^{2+}, Cd^{2+}, Zn^{2+} and Pb^{2+} [35-37]. For example, Liang et al. [38, 39] applied thiol-functionalized sepiolite and palygorskite to enhance the immobilisation of Cd and successfully reduced the bioavailability of Cd through plant physiological and soil chemistry mechanisms. In another study, Huang et al.[40] successfully reduced by more than 90% extractable Hg using thiol-functionalized graphene oxide/Fe-Mn composite.

Several studies concerning biochar modified with thiol groups have been published. Xia et al. (2019) produced thiol modified biochar using 3-mercaptopropyltrimethoxysilane(3-MPTS), and reported thiol modification to increase adsorption capacity for Hg[41, 42]. However, this adsorption capacity was lower than that of thiol modified active carbon or thiol modified

graphene oxide. Huang et al. (2019) reported that thiol-functionalized biochar effectively removed Hg^{2+} and CH_3Hg^+ from solution, and that natural organic matter (NOM), glucose and humic acid (up to 24 mg/L) had little effect on the adsorption[41, 42].

However, most of these studies on thiol-functionalized biochar are still limited, particularly for typical soil metal pollutants such as Cd^{2+} and Pb^{2+}. In addition, previous research has mainly focus on the performance of thiol-functionalized biochar on metal adsorption in solution rather than under genuine soil conditions. Here we adopt a simple and novel path, using β-mercaptoethanol, to prepare a thiol-modified rice biochar and assess its efficacy for enhancing the remediation of soils contaminated with Cd and Pb. Specifically, the properties of thiol modified biochar (RS) were characterized to investigate their influence on the adsorption of Cd and Pb present in water and in soil (both individually and as binary mixtures).

2 Materials and methods

2.1 Rice straw biochar and thiol-modified biochar production and characterization

Before charring, rice straw was collected, air-dried and cut to lengths less than 2cm. Rice straw biochar (RB) was produced by slowly pyrolysis under N_2 in a muffle furnace (KSL, Kejing Inc., China). The furnace was heated to 500°C at a heating rate of 20°C min^{-1} and held at this temperature for 5 h. Then biochar samples were collected, crushed and ground to pass through a 60-mesh sieve.

In brief, thiol-modification was achieved as follows: 1 g of RB was placed in a brown glass bottle with 4 mL of β-mercaptoethanol (>99%, AR), acetic anhydride (>98.5, AR, 2.8 mL) and concentrated sulphuric acid (>95.0%, AR, 0.2 mL) were then added. The bottle was then sealed and shaken for 18 h at 80 °C. After filtration, the product was washed thoroughly with ultrapure water and then dried in a vacuum oven for 12 h at 35 °C. Thereafter, the product (RS) was crushed and ground to pass through a 60-mesh sieve.

pH was measured using a pH meter (STARTER 3100/F, Ohaus Inc., China) at the ratio of 1 g biochar: 20 mL ultrapure water. The content of thiol group on biochar was analyzed using Ellman reagent[43]. Briefly, biochar (2 mg) was suspended in ethanol (0.2 mL) using ultrasound. Thereafter, 0.2 mol L^{-1} phosphate buffered solution (PBS, pH 7.8, 1 mL) and 5,5'-dithiobis-(2-nitrobenzoic acid) solution (2g L^{-1} in PBS, 0.2 mL) were added to the biochar suspension. After 5 min of incubation, the solution was filtered and the absorbance at 412 nm was measured. Carbon, nitrogen, and sulphur content were determined using a CNS elemental analyzer (Vario Max, Elementar Analysensysteme GmbH Inc., German). The pH_{pzc} was measured according to the protocol reported by Mohan et al[44]. The morphologies and surface features were characterized by a field emission scanning electron microscope (FE-SEM) (S-4800, Hitachi Inc., Japan). The specific surface area and pore size distribution were determined by Brunauer-Emmett-Teller (BET) and Barret-Joyner-Halenda (BJH) methods with N_2 adsorption isotherms, respectively. Fourier transform infrared (FT-IR) (Thermo Scientific Nicolet iS10, Thermo Fisher Scientific Inc., USA) analysis was carried out over a range of 400 - 4000 cm^{-1} using the

KBr pellet technique. X-ray photoelectron spectroscopy (XPS) analysis was determined using a spectrophotometer (*K-Alpha*$^{+}$, Thermo Fisher Scientific Inc., USA) with an Al Kα source (1486.6 eV of photons).

2.2 Batch sorption experiment

Batch adsorption experiments were conducted to investigate the adsorption characterization of RB and RS. Both single- (either Cd^{2+} or Pb^{2+}) and binary- (both Cd^{2+} and Pb^{2+}) metal adsorption experiments were conducted to determine the sorption capacities of RB and RS in a buffered aqueous system (pH 5, 0.05 mol L^{-1} acetic acid). Briefly, 25 mg of RB or RS were added to centrifuge tubes containing 10 mL of single metal ion (Cd^{2+} or Pb^{2+}) solutions or binary metal ion solutions (the mass ratio of Cd^{2+} to Pb^{2+} was 1:1) of various initial concentrations (50 - 600 mg L^{-1}). The centrifuge tubes were shaken (180 rpm for 24 h) and the suspension was filtered through a 0.22 μm membrane filter. After filtration, the concentrations of heavy metals in the filtrate were determined by an inductively coupled plasma optical emission spectrometer (ICP-OES) (Optima, Perkin Elmer Inc., America). Sorption kinetic experiments of Cd^{2+} and Pb^{2+} on RB and RS were carried using 250 mL conical flasks, containing 100 mL of 200 mg L^{-1} single metal ions (Cd^{2+} or Pb^{2+}) solutions buffered to pH 5 (0.05 mol L^{-1} acetic acid), and flasks were sampled periodically (0 - 24h). The effect of pH on sorption of metal ion (Cd^{2+} or Pb^{2+}) was determined using solutions of 50 mg L^{-1} concentrations

of metal ion adjusted to the desired pH (2 - 7). All the adsorption experiments were conducted in triplicate.

2.3 Soil incubation experiments

A soil sample from the surface layer (0 - 20 cm) was collected from a contaminated vegetable field in Longyan (Fujian Province, China). The soil sample was air dried and passed through a 2-mm sieve. Soil physicochemical properties are reported in Table 1. The concentration of soil Cd and Pb were 9.18 and 1182 mg kg^{-1}, respectively. Both metals were present in soil above the risk intervention values published by the government of China[45] for agricultural land (3.0 mg kg^{-1} for Cd and 700 mg kg^{-1} for Pb).

The soil incubation experiments were performed with soil (30 g) enclosed in the 50 mL centrifuge tube. Dosages of 0, 1%, and 3% RB or RS were homogenously mixed into the soil. Thus, the incubation experiment included five treatments: Soil (CK), Soil + 1% RB (RB-1%), Soil + 3% RB (RB-3%), Soil + 1% RS (RS-1%) and Soil + 3% RS (RS-3%). All the mixtures were incubated at 80% water holding capacity at 25 °C. Two batches of samples were prepared for destructive sampling after incubation time of 7 and 28 days. At the designated time, soil samples were air dried, and passed through a 2-mm sieve. Three replicates of each treatment were performed. Soil pH, cation exchange capacity (CEC) and organic matter (O.M) were measured. The available Cd and Pb concentrations of soil samples were estimated by diethylenetriaminepentaacetic acid (DTPA) solution extraction[46, 47]. Chemical fractionation

of Cd and Pb were determined using a sequential extraction procedure[48]. The fractions included exchangeable fraction (EX), carbonate-bound fraction (CB), Fe/Mn oxides-bound fraction (OX), organic matter-bound fraction (OM) and residual fraction (RES). The metal concentrations in the extracts were detected using ICP-MS (Agilent 7500cx, Agilent, America).

3 Results and discussion

3.1 Physicochemical properties

Physicochemical properties of RB and RS are presented in Table 2. The elemental analysis revealed that the composition of RS was markedly changed after thiol-modification. The nitrogen content and carbon content of RS were lower than RB. The sulphur content of RS was 24.04% (while it was only ~1% in RB). The accessible thiol contents, putatively available for heavy metal adsorption, were 0.83 and 0.01 mmol g^{-1} for RS and RB, respectively. The increased sulphur content and accessible thiol contents of RS confirmed that thiol groups had been successfully introduced. After thiol-modification, the pH and pH_{pzc} of RS decreased dramatically with respect to RB. As the pH of biochar is mainly affected by surface functional groups[49], the decrease of pH of RS indicated that thiol-modification increased acidic functional groups on the surface of RS. The low pH_{pzc} of RS suggested that the incorporation of thiol groups led to an enhancement of surface negative charges (these will have likely influenced adsorption of metal cations favorably[50]).

The surface area of RS decreased from 7.82 m^2 g^{-1} to 0.34 m^2 g^{-1} and pore diameter of RS decreased from 20.8 nm to 16.7 nm due to infilling of the pores with thiol groups[43]. Fig. S1 shows typical FE-SEM images of RB and RS. RB had regular pore structure with rough surface and some particles attached. After thiol-modification, the surface of RS was covered with a layer of smooth membranous material and the pores were visually observed to be blocked. These observations are consistent with previous reports that pore blockage caused by grafting of the thiol groups[43, 51].

To identify the chemical changes of the functional groups on the adsorbent surface, FT-IR spectra were obtained (Fig. 1). In the RB spectrum, the peaks at 1573, 1419, 1066, 617 and 459 cm^{-1} were attributed to the vibration of C=O/C=C, C-OH (phenolic), C–O (carboxylic), C-O (alkyl), and C-C, respectively[52-57]. Comparing the spectra before and after thiol-modification, the spectrum of RS changed obviously. In the RS spectrum, the broad adsorption peak at 3446 cm^{-1} was ascribed to the O-H stretching vibrations. New peaks observed at 1233 cm^{-1} and 1028 cm^{-1} were attributed to the lactones and the stretching vibration of C–O[58, 59], respectively. The peaks observed at 2929 and 2560 cm^{-1} corresponded to the -CH_2- vibrations of β-mercaptoethanol and thiol group, respectively[35, 60]. These results confirmed that the β-mercaptoethanol was successfully introduced on the biochar support. The adsorption band at 1739 cm^{-1} was assigned to ester carbonyl stretching[61], while the peak at 1066 cm^{-1} belonging to carboxylic acids markedly reduced[55]. These results confirmed the β-mercaptoethanol grafting had been achieved via ester linkages. The peak at 671 cm^{-1} was assigned to C–S [62].

It also confirmed the presence of β-mercaptoethanol. Additionally, the FT-IR spectra showed that sulfonic groups were not formed during thiol-modification of RS although there was concentrated H_2SO_4 addition during the preparation. The vibration band at 1040 cm^{-1} (attributed to S=O symmetric stretching) indicating the presence of sulfonic groups, was not visible in the FT-IR spectrum. The absence of this band in the FT-IR spectra confirmed the absence of $-SO_3H$ groups on thiol-modified RS[63]. In summary, the β-mercaptoethanol was successfully introduced onto RS by esterification (see reaction route presented in Fig. 2)[35, 64].

3.2 Sorption of Cd and Pb from aqueous solution

3.2.1 Sorption kinetics

The adsorption of Cd^{2+} on RB was observed to be slow. The equilibrium was achieved after approximately 24 h (Fig. 3a). The adsorption rate of Cd^{2+} on RS initially increased rapidly, and then decreased to reach an equilibrium within 2 h. The equilibrium adsorption capacity of RS was three times higher than that of RB.

In order to probe the sorption mechanisms, the sorption kinetics data were fitted using a pseudo-first-order kinetic model and a pseudo-second-order kinetic model (Table 3). Cd^{2+} sorption kinetics on RB was better described by the pseudo-first-order kinetic model. This suggested that mononuclear sorption of Cd^{2+} was underpinning sorption by RB[65]. In contrast, the pseudo-second-order kinetic model better fitted the kinetic data of Cd^{2+} on RS, suggesting

that the rate-limiting step was chemical sorption. As shown in Fig. 3b, the adsorption of Pb^{2+} on RB was initially more rapid than its adsorption on RS, and thereafter decreased considerably with the extension of time until equilibrium was achieved. Pb^{2+} adsorption by RB and RS was better described by the pseudo-second-order kinetic models, suggesting that the rate-limiting step was chemical sorption. These results demonstrated that, in comparison to RB, RS had a large affinity for Cd^{2+} and relatively low affinity to Pb^{2+}, while RB had a high affinity for Pb^{2+} and a far lower affinity for Cd^{2+}.

3.2.2 Sorption isotherms of Cd and Pb in single- and binary-metal systems

The adsorption isotherms of Cd^{2+} and Pb^{2+} on RB and RS in the single-metal systems are provided in Fig. 4, and the model parameters fitted by the Langmuir and Freundlich models are listed in Table 4. The adsorption capacities of RB for Cd^{2+} were greatly enhanced, while the adsorption capacities of RB for Pb^{2+} were slightly decreased after thiol-modification.

For Cd^{2+}, the maximum adsorption capacity on RS was 45.1 mg g^{-1}, 3-fold higher than that of RB. For Pb^{2+}, the maximum adsorption capacities on RB and RS were 67.4 and 61.4 mg g^{-1}, respectively. Correlation coefficients indicated that the Langmuir model fitted adsorption isotherms of Cd^{2+} and Pb^{2+} on RB and RS better than the Freundlich model. This observation suggests that metal ion adsorption occurred at a homogeneous surface by monolayer sorption without interaction between the adsorbed ions[66].

The increase in adsorption capacity of RS for Cd^{2+} was ascribed to the incorporation of thiol

groups on RS. The characteristic band of thiol groups at 2560 cm^{-1} in the FT-IR spectra of RS-Cd^{2+} disappeared after adsorption (Fig. S2); this indicated the interactions between thiol groups and Cd^{2+} or Pb^{2+}[67]. The lone pair of electrons on the sulphur atoms of the thiol groups have been reported to coordinate with heavy metals, thus promoting their adsorption[35].

However, the adsorption capacity of RS for Pb^{2+} was slightly decreased when compared to RB. This result might be attributed to the significant reduction in carboxylic groups remaining on RS following thiol groups; these carboxylic groups act as reaction sites for the esterification (Fig. 2). It can be inferred that in the adsorption of heavy metals, the main adsorption sites on RB were oxygen-containing functional groups (such as carboxyl groups), while the thiol groups on RS played a great role. Comparing the FT-IR spectra of RB before and after Cd^{2+} or Pb^{2+} adsorption (Fig. S2), the shift of carboxylic group related band at 1066 cm^{-1} suggest the binding of metal ions with carboxylic groups on RB[55]. In addition, the disappearance of O1s peaks at 534.2 eV (Fig. S3) and the shift of C1s peak at 288.0 eV (Fig. S4) also indicate that the carboxyl groups on RB were involved in adsorption[68, 69]. However, the carboxyl groups were markedly reduced after thiol-modification, as confirmed by FT-IR spectra (Fig. 1) and XPS O1s spectra (Fig. S3)[70]. According to Lewis' HSAB (hard and soft acids and bases) theory, soft acids (acceptors) tend to form strong bonds with soft bases (donors), but bind reluctantly or weakly to harder bases, while hard acids (acceptors) tend to form strong bonds with hard bases (donors), but bind reluctantly or weakly to softer bases[71]. Carboxyl groups (a hard base) are more

favorable to adsorb Pb^{2+} (Pb^{2+} is a borderline acid while Cd^{2+} is a soft acid) [72]. In contrast, the interaction between thiol groups (soft base) and Cd^{2+} is more favorable compared to Pb^{2+} [69]. Therefore, although the content of thiol groups on RS was increased, the loss of carboxylic groups during the thiol-modification lead to the slight decrease of adsorption capacity of Pb^{2+}. As shown in Fig. 5, the maximum adsorption capacity of Cd^{2+} and Pb^{2+} on RB and RS decreased considerably in the binary-metal system compared to in the single-metal system. Competition between Cd^{2+} and Pb^{2+} in the binary-metal systems was well fitted by the Langmuir model (Table 5). The decreasing amplitude of Cd^{2+} adsorption on RB caused by competition was larger than the decreasing amplitude of Pb^{2+} adsorption. The decreases in adsorption capacities of RB for Cd^{2+} and Pb^{2+} were 52% and 6%, respectively. In contrast, the decreases in adsorption capacities of RS for Cd^{2+} and Pb^{2+} were 10% and 51%, respectively. Furthermore, the distribution coefficient (K_d) illustrated clearly the adsorption preference for Cd^{2+} and Pb^{2+} on RB and RS (Table 6). RB showed more prominent selectivity for Pb^{2+} over Cd^{2+}. On the contrary, RS had adsorption selectivity for Cd^{2+} over Pb^{2+}. The adsorption preference for Pb^{2+} by biochar has been reported in other studies. Park[72] found that sesame straw biochar adsorbed more Pb^{2+} from a multi-metal system (of Pb^{2+}, Cu^{2+}, Cr^{2+}, Zn^{2+} and Cd^{2+}). This might be attributed to the lower hydrated radius of Pb^{2+} and greater affinity of Pb^{2+} for most functional groups, including phenolic and carboxylic groups (hard Lewis bases), on the sesame straw biochar. A reasonable explanation for the observation in our experiments is that thiol groups (soft Lewis bases) had higher affinity for cadmium ions (soft Lewis acids)[73].

3.2.3 Effects of pH on sorption

pH is a crucial parameter in adsorption processes as it can affect the surface charge of adsorbents and metal speciation[74]. Changes in the initial pH of the adsorbent/solution systems affected Cd^{2+} and Pb^{2+} adsorption by RB and RS (Fig. S5). In general, the removal efficiency of the metals by RB and RS increased with increasing pH until reaching a plateau. The removal of Cd^{2+} by RS was much higher than RB with the increase of pH from 2 to 4. The removal of Cd^{2+} by RS remained constant above pH 5 while it continued to increase with RB. In contrast, the removal of Pb^{2+} by both RB and RS increased with increasing pH. These phenomena were likely due to the presence of a large number of H^+ and H_3O^+ ions in aqueous solution at low pH (these ions competing with the metal ions for adsorption sites). With increasing pH, the competition between metal ions and protons for binding sites decreased and more binding sites were released[75]. Furthermore, the surface charge of the adsorbent would be positive below the pH_{PZC} or be negative above the pH_{PZC}. While solution pH exceeds pH_{PZC}, the negative surface charge on adsorbent increase with the increase of solution pH and therefore shows better heavy metal removal efficiency at higher pH[76]. These observations suggest that ion exchange mechanisms underpin the adsorption of Cd^{2+} and Pb^{2+} on RB and RS[55].

3.2.4 Sorption mechanism

To further elucidate the mechanism of Cd^{2+} and Pb^{2+} adsorption onto RS and RB, XPS data

were collected (Fig. 6). Fig. 6a showed S2p spectrum of sulphur of RS before and after adsorption of Cd^{2+} and Pb^{2+}. The S2p binding energy of RS at 162.9 eV and 164.0 eV were ascribed to the grafted thiol monolayers and thiol group[77]. For Cd^{2+}- and Pb^{2+}-laden RS, the decrease in thiol groups from 42% to 29% and 27%, were ascribed to the interactions between thiol groups and Cd^{2+} or Pb^{2+}, respectively. Similarly, Huang et al. (2019) found that thiol groups on thiol-functionalized graphene oxide/Fe-Mn composite decreased by 30% and 10%, respectively, after Hg^{2+} and CH_3Hg^+ adsorption, indicating surface complexation[78]. Fig. 6b indicates $Cd3d_{3/2}$ (412.3 eV) and $Cd3d_{5/2}$ (405.5 eV) binding energies that suggest the formation of precipitates, such as cadmium hydroxide and carbon oxides, associated with the adsorption of Cd^{2+}[79]. From Fig. 6c, two peaks at 411.4 and 404.6 eV of RS, assigned to $Cd3d_{3/2}$ and $Cd3d_{5/2}$ of Cd^{2+} in CdS[80], indicated that cadmium species were adsorbed via binding reactions between cadmium ions and thiol groups. For the spectrum of Pb4f of Pb loaded RB (Fig. 6d), the binding energies of 144.7 eV for $Pb4f_{5/2}$, and 139.8 eV for $Pb4f_{7/2}$ suggest the complexation of PbO[81]. From Fig. 6e it can be seen that the Pb4f spectrum of Pb loaded RS had $Pb4f_{7/2}$ binding energy at 137.4 eV and $Pb4f_{5/2}$ binding energy at 142.3 eV; these are in good agreement with data obtained for PbS[82]. The interactions between thiol groups and metal ions played an important role in the adsorption of Pb^{2+} onto RS. Collectively, these results showed that after thiol-modification surface complexation reactions involving grafted thiol groups and metal ions facilitated their adsorption/precipitation[42, 83].

3.3 Remediation of Cd and Pb in soil

3.3.1 Effects on soil pH, O.M and CEC

The influence of RB and RS on soil pH, O.M and CEC was assessed (Fig. S6). These attributes are important influencers of heavy metal behaviour in soil.

Compared with the control soil (pH 7.42), RB addition to soil resulted in a significant ($p < 0.05$) increase in pH (Fig. S6a). In contrast, RS addition significantly decreased soil pH ($p < 0.05$). Across all the incubation times, RB increased the pH of soil by 0-0.49 units and the addition of RS decreased the pH of soil by 0.07-0.36 units across all the incubation times. No time-related trends in pH were observed over the 28 days. However, significant ($p < 0.05$) relationships between pH and increasing RB/RS application doses were observed. The high pH RB (pH = 10.2) likely underpinned increases in soil pH[84]. The decrease of soil pH after addition of RS was likely caused by the acidity of RS (pH = 2.4).

With increasing application, RB and RS significantly increased soil O.M compared to the CK (Fig. S6b) ($p < 0.05$). The soil O.M increased respectively by 28-115% and 33-130% following RB and RS addition (28 days). There was no significant difference observed between RB and RS on soil O.M ($p > 0.05$). The addition of biochar to soil has previously been reported to significantly increase the content of soil O.M due to its high carbon content[85].

The addition of RB and RS, across all incubation periods, resulted in a slight but insignificant enhancement of CEC compared with the control (Fig. S6c) ($p > 0.05$). As the effect of biochar

on soil CEC has been reported to related to the incubation time[86], the insignificant effect of RB/RS on soil CEC may be linked to the short period of incubation used in this study.

3.3.2 Effects on availability of Cd and Pb

The effect of RB/RS on the concentration of available Cd and Pb in the soil was determined by DTPA extraction (Fig. 7). These results revealed that available Cd in RB treated soils and RS treated soils were lower than in CK soil. The influence of RB treatment on available Cd content were not significant ($p > 0.05$), except RB-3% at day 28. In comparison, RS had a greater immobilization effect than RB; available Cd content in all RS treated soils decreased significantly ($p < 0.05$) by 17.5-27.7% (day 7) and 34.8-39.2% (day 28), respectively. The available Pb content in soil fluctuated with the addition of RB and RS at day 7. After day 28, the available Pb decreased between 10 and 19% in RB treated soils) and between 9 and 11% in RS treated soils. There was however no significant difference compared with CK ($p > 0.05$). Biochar has been reported to mainly influences the mobility of heavy metals by changing CEC and pH of soil[87]. In this study, RB had no significant effect on soil CEC. On the other hand, RB significantly increased soil pH (but by less than 0.5 pH units). It has been reported that the pH changes of biochar added to alkaline soil (as is the case in this research) had no significant correlation with the availability of heavy metals[25]. These two reasons might lead to poor immobilization effect of RB on Cd and Pb. Unlike other pH-regulating immobilization agents such as biochar and lime, RS addition decreased the soil pH. The thiol groups grafted onto RS

enhanced the retention of Cd in soil through the formation of metal complexes and thus the availability of heavy metals was decreased[18]. Similarly, He et al.(2018) suggested thiol groups grafted onto palygorskite (MP) decreased available Cd in soil by 90%, and reduced Cd concentrations in pak choi[88]. Thiol groups on MP were reported to directly adsorb metal ions from soil. In addition, MP also changed soil properties including surface zeta potential, which increased the chemical reaction between soil and Cd. Lian et al.(2019) reported that thiol functionalized reactive nanosilica reduced soil bioavailable-Cd from 12.46 mg/kg to 0.22 mg/kg, and most Cd was transformed into more stable species due to the chemical reaction between Cd and thiol groups[89]. In this study, the addition of RS shifted the phytoavailable Cd fractions (EX and CB fractions) to the less available fractions (OX and OM fractions) (see section 3.3.3). For Pb, there was limited immobilization effect for RS or RB. This was likely due to the high concentration of Pb in the soil.

3.3.3 Influence of RB and RS on Cd and Pb speciation in soils

The speciation of Cd and Pb in soils are shown in Fig. 8. Cd was mainly bound to exchangeable, carbonate-bound and Fe/Mn oxides-bound fractions, the sum of the three fractions accounted to more than 90% of total Cd in CK. Pb mainly existed in Fe/Mn oxides-bound and residual fractions, and the sum of the two fractions accounts for more than 80% of total Pb in CK. In the CK soil, 57-62% of Cd and 7-14% of Pb were found in the exchangeable and carbonate-

bound fractions. These fractions have previously been reported as the phytoavailable fractions of heavy metal in soil[90, 91].

Over the 28-day period, the application of RB did not have any obvious influence on Cd speciation in soil. RB decreased phytoavailable Cd of total Cd by 2 and 5%, respectively. In contrast, additions of RS shifted Cd species from the carbonate fraction to the Fe/Mn oxide fraction. Carbonate-bound fractions of Cd decreased by 5 and 13% following RS application, while the percentages of Fe/Mn oxides-bound fractions of total Cd increased by 9 and 16%. Thus, RS treatment decreased phytoavailable Cd between 10 and 14%. The RB and RS treatment did not have a significant influence on Pb speciation during the incubation. The percentages of phytoavailable Pb of total Pb decreased between 1 and 4%, 1 and 6% after RB and RS application, respectively.

Biochar can not only directly reduce the available content of heavy metals in soil by means of adsorption or precipitation, but it can also indirectly reduce the available content of heavy metals in soil by altering pH, electrical conductivity and other soil properties[92, 93]. However, in this study, RB had limited immobilization effect on both Cd and Pb in the soil. Addition of thiol-modified sepiolite to Cd contaminated farmland soil has been reported transform the exchangeable fraction and carbonate-bound fraction of Cd into the Fe/Mn oxides-bound fraction, organic matter-bound fraction and residual fraction[38]. The increase of Fe/Mn oxides-bound fractions of Cd have been reported to be underpinned by the adsorption of Cd on Fe/Mn oxides-bound indirectly promoted by thiol-modified sepiolite; while the increase of organic

matter-bound fractions of Cd have been reported to be due to the adsorption of Cd by thiol functional groups directly. In this study, RS had a better immobilization effect on Cd in the soil and the addition of RS transformed carbonate-bound fraction of Cd into Fe/Mn oxides-bound fractions. A reasonable explanation is that the carbonate-bound fraction of Cd, which may have been solubilize under acidic conditions[94], released Cd into the soil solution as the pH decreased following RS addition; and, these released Cd ions were re-adsorbed by thiol functional groups on RS[40]. In contrast to Cd, RS had negligible impacts on the chemical fraction of Pb in the soil. This contrast in fractionation outcome likely influenced the adsorption selectivity of RS for Cd over Pb. However, the extreme high level of Pb contamination (1182 mg kg^{-1}) in soil might be the main reason for the limited immobilization effect observed.

4 Conclusions

Thiol-modified biochar was successfully prepared by esterification with β-mercaptoethanol. The kinetics of adsorption of Cd^{2+} and Pb^{2+} on RS were found to be rapid, and the experimental data was well described by pseudo-second order kinetics; indicating that the adsorption was controlled by chemisorption. The thiol-modification tripled the sorption capacity for Cd^{2+} and slightly decrease the sorption capacity for Pb^{2+}. Cd^{2+} and Pb^{2+} were removed mainly via surface complexation. The RS exhibited an adsorption preference for Cd^{2+} over Pb^{2+} in binary-metal systems. The laboratory-scale incubation test showed that RS had better performance than RB

in immobilizing Cd and shifting Cd to less phytoavailable fractions in the soil. Both RB and RS significantly increased the organic matter content of soil and slightly increase cation exchange capacity in the soil. These results suggest RS could be a useful material for the remediation for heavy metal contamination in water and soil. Further studies should be conducted to provide more understanding of the interaction between thiol groups on RS and metal ions. Furthermore, the effects of RS on metal mobility under field conditions, with crops present, need to be established.

Acknowledgements

The current study was supported by the National key R&D Project (2018YFC1802703), the Natural Science Foundation of China (41501525), the Science and Technology Project of Fujian province (2018N0033) and the Science and Technology Project of Xiamen city (3502Z20182001).

References

[1] Huang Y, Wang L, Wang W, et al. Current status of agricultural soil pollution by heavy metals in China: a meta-analysis. Science of the Total Environment, 2019, 651, 3034-3042. https://doi.org/10.1016/j.scitotenv.2018.10.185

[2] Gasperi J, Ayrault S, Moreau-Guigon E, et al. Contamination of soils by metals and organic micropollutants: case study of the Parisian conurbation. Environmental Science and Pollution Research, 2018, 25(24), 23559-23573. https://doi.org/10.1007/s11356-016-8005-2

[3] Yang Q, Li Z, Lu X, et al. A review of soil heavy metal pollution from industrial and agricultural regions in China: pollution and risk assessment. Science of the Total Environment, 2018, 642: 690-700. https://doi.org/10.1016/j.scitotenv.2018.06.068

[4] Cai L M, Wang Q S, Luo J, et al. Heavy metal contamination and health risk assessment for children near a large Cu-smelter in central China. Science of the Total Environment, 2019, 650: 725-733. https://doi.org/10.1016/j.scitotenv.2018.09.081

[5] China's Ministry of Environmental Protection. National soil pollution survey bulletin. China's Ministry of Environmental Protection, 2014. http://www.mee.gov.cn/gkml/sthjbgw/qt/201404/t20140417_270670.htm.

[6] Shi T, Ma J, Zhang Y, et al. Status of lead accumulation in agricultural soils across China (1979–2016). Environment international, 2019, 129: 35-41. https://doi.org/10.1016/j.envint.2019.05.025

[7] Abad-Valle P, Álvarez-Ayuso E, Murciego A, et al. Assessment of the use of sepiolite amendment to restore heavy metal polluted mine soil. Geoderma, 2016, 280: 57-66. http://dx.doi.org/10.1016/j.geoderma.2016.06.015

[8] Sun Y, Sun G, Xu Y, et al. Evaluation of the effectiveness of sepiolite, bentonite, and phosphate amendments on the stabilization remediation of cadmium-contaminated soils. Journal of Environmental Management, 2016, 166: 204-210. http://dx.doi.org/10.1016/j.jenvman.2015.10.017

[9] Chu W. Remediation of contaminated soils by surfactant-aided soil washing. Practice Periodical of Hazardous, Toxic, and Radioactive Waste Management, 2003, 7(1): 19-24. https://doi.org/10.1061/(ASCE)1090-025X(2003)7:1(19)

[10] Sierra M J, Millan R, Lopez F A, et al. Sustainable remediation of mercury contaminated soils by thermal desorption. Environmental Science and Pollution Research International, 2016, 23(5): 4898-4907. https://doi.org/10.1007/s11356-015-5688-8

[11] Tauqeer H M, Ali S, Rizwan M, et al. Phytoremediation of heavy metals by

Alternanthera bettzickiana: growth and physiological response. Ecotoxicology and Environmental Safety, 2016, 126: 138-146. http://dx.doi.org/10.1016/j.ecoenv.2015.12.031

[12] Rizwan M, Ali S, Zia Ur Rehman M, et al. Cadmium phytoremediation potential of *Brassica* crop species: a review. Science of the Total Environment, 2018, 631-632: 1175-1191. https://doi.org/10.1016/j.scitotenv.2018.03.104

[13] Peng W, Li X, Song J, et al. Bioremediation of cadmium- and zinc-contaminated soil using *Rhodobacter sphaeroides*. Chemosphere, 2018, 197: 33-41. https://doi.org/10.1016/j.chemosphere.2018.01.017

[14] Mishra J, Singh R, Arora N K. Alleviation of heavy metal stress in plants and remediation of soil by rhizosphere microorganisms. Frontiers in Microbiology, 2017, 8: 1706. https://doi.org/10.3389/fmicb.2017.01706

[15] Liang Y, Cao X, Zhao L, et al. Biochar- and phosphate-induced immobilization of heavy metals in contaminated soil and water: implication on simultaneous remediation of contaminated soil and groundwater. Environmental Science and Pollution Research International, 2014, 21(6): 4665-4674. https://doi.org/10.1007/s11356-013-2423-1

[16] Barbosa B, Boléo S, Sidella S, et al. Phytoremediation of heavy metal-contaminated soils using the perennial energy crops *Miscanthus* spp. and *Arundo donax* L. BioEnergy Research, 2015, 8(4): 1500-1511. https://doi.org/10.1007/s12155-015-9688-9

[17] Wuana R A, Okieimen F E. Heavy metals in contaminated soils: a review of sources, chemistry, risks and best available strategies for remediation. ISRN Ecology, 2011, 2011: 1-20. https://doi.org/10.5402/2011/402647

[18] Zhang L, Shang Z, Guo K, et al. Speciation analysis and speciation transformation of heavy metal ions in passivation process with thiol-functionalized nano-silica. Chemical Engineering Journal, 2019, 369: 979-987. https://doi.org/10.1016/j.cej.2019.03.077

[19] Wang L, Chen L, Cho D W, et al. Novel synergy of Si-rich minerals and reactive MgO for stabilisation/solidification of contaminated sediment. Journal of Hazardous Materials,

2019, 365: 695-706. https://doi.org/10.1016/j.jhazmat.2018.11.067

[20] O'connor D, Peng T, Zhang J, et al. Biochar application for the remediation of heavy metal polluted land: a review of *in situ* field trials. Science of the Total Environment, 2018, 619-620: 815-826. https://doi.org/10.1016/j.scitotenv.2017.11.132

[21] Liu L, Li W, Song W, et al. Remediation techniques for heavy metal-contaminated soils: principles and applicability. Science of the Total Environment, 2018, 633: 206-219. https://doi.org/10.1016/j.scitotenv.2018.03.161

[22] Bian R J, Chen D, Liu X Y, et al. Biochar soil amendment as a solution to prevent Cd-tainted rice from China: results from a cross-site field experiment. Ecological Engineering, 2013, 58: 378-383. http://dx.doi.org/10.1016/j.ecoleng.2013.07.031

[23] Lu K, Yang X, Gielen G, et al. Effect of bamboo and rice straw biochars on the mobility and redistribution of heavy metals (Cd, Cu, Pb and Zn) in contaminated soil. Journal of Environmental Management, 2017, 186: 285-292. http://dx.doi.org/10.1016/j.jenvman.2016.05.068

[24] Cui H, Fan Y, Fang G, et al. Leachability, availability and bioaccessibility of Cu and Cd in a contaminated soil treated with apatite, lime and charcoal: a five-year field experiment. Ecotoxicology and Environmental Safety, 2016, 134: 148-155. http://dx.doi.org/10.1016/j.ecoenv.2016.07.005

[25] Zhang G, Guo X, Zhao Z, et al. Effects of biochars on the availability of heavy metals to ryegrass in an alkaline contaminated soil. Environmental Pollution, 2016, 218: 513-522. http://dx.doi.org/10.1016/j.envpol.2016.07.031

[26] Peng H, Gao P, Chu G, et al. Enhanced adsorption of Cu(II) and Cd(II) by phosphoric acid-modified biochars. Environmental Pollution, 2017, 229: 846-853. http://dx.doi.org/10.1016/j.envpol.2017.07.004

[27] Jin H, Capareda S, Chang Z, et al. Biochar pyrolytically produced from municipal solid wastes for aqueous As(V) removal: adsorption property and its improvement with KOH

activation. Bioresource Technology, 2014, 169: 622-629. http://dx.doi.org/10.1016/j.biortech.2014.06.103

[28] Zhang M, Gao B, Varnoosfaderani S, et al. Preparation and characterization of a novel magnetic biochar for arsenic removal. Bioresource Technology, 2013, 130: 457-462. http://dx.doi.org/10.1016/j.biortech.2012.11.132

[29] Liang J, Li X, Yu Z, et al. Amorphous MnO_2 modified biochar derived from aerobically composted swine manure for adsorption of Pb(II) and Cd(II). ACS Sustainable Chemistry & Engineering, 2017, 5(6): 5049-5058. https://doi.org/10.1021/acssuschemeng.7b00434

[30] Zuo W Q, Chen C, Cui H J, et al. Enhanced removal of Cd(II) from aqueous solution using $CaCO_3$ nanoparticle modified sewage sludge biochar. RSC Advances, 2017, 7(26): 16238-16243. https://doi.org/10.1039/c7ra00324b

[31] Yu J, Jiang C, Guan Q, et al. Enhanced removal of Cr(VI) from aqueous solution by supported ZnO nanoparticles on biochar derived from waste water hyacinth. Chemosphere, 2018, 195: 632-640. https://doi.org/10.1016/j.chemosphere.2017.12.128

[32] Xue Y W, Gao B, Yao Y, et al. Hydrogen peroxide modification enhances the ability of biochar (hydrochar) produced from hydrothermal carbonization of peanut hull to remove aqueous heavy metals: batch and column tests. Chemical Engineering Journal, 2012, 200: 673-680. http://dx.doi.org/10.1016/j.cej.2012.06.116

[33] Zhou Y, Gao B, Zimmerman A R, et al. Sorption of heavy metals on chitosan-modified biochars and its biological effects. Chemical Engineering Journal, 2013, 231: 512-518. https://doi.org/10.1016/j.cej.2013.07.036

[34] Yang G X, Jiang H. Amino modification of biochar for enhanced adsorption of copper ions from synthetic wastewater. Water Research, 2014, 48: 396-405. http://dx.doi.org/10.1016/j.watres.2013.09.050

[35] Chai L, Li Q, Zhu Y, et al. Synthesis of thiol-functionalized spent grain as a novel adsorbent for divalent metal ions. Bioresource Technology, 2010, 101(15): 6269-6272. https://doi.org/10.1016/j.biortech.2010.03.009

[36] Zhang C, Sui J H, Li J, et al. Efficient removal of heavy metal ions by thiol-functionalized superparamagnetic carbon nanotubes. Chemical Engineering Journal, 2012, 210: 45-52. http://dx.doi.org/10.1016/j.cej.2012.08.062

[37] Jiang L, Li S, Yu H, et al. Amino and thiol modified magnetic multi-walled carbon nanotubes for the simultaneous removal of lead, zinc, and phenol from aqueous solutions. Applied Surface Science, 2016, 369: 398-413. http://dx.doi.org/10.1016/j.apsusc.2016.02.067

[38] Liang X F, Qin X, Huang Q Q, et al. Mercapto functionalized sepiolite: a novel and efficient immobilization agent for cadmium polluted soil. RSC Advances, 2017, 7(63): 39955-39961. https://doi.org/10.1039/c7ra07893e

[39] Liang X, Qin X, Huang Q, et al. Remediation mechanisms of mercapto-grafted palygorskite for cadmium pollutant in paddy soil. Environmental Science and Pollution Research International, 2017, 24(30): 23783-23793. https://doi.org/10.1007/s11356-017-0014-2

[40] Huang Y, Wang M, Li Z, et al. *In situ* remediation of mercury-contaminated soil using thiol-functionalized graphene oxide/Fe-Mn composite. Journal of Hazardous Materials, 2019, 373: 783-790. https://doi.org/10.1016/j.jhazmat.2019.03.132

[41] Xia S, Huang Y, Tang J, et al. Preparation of various thiol-functionalized carbon-based materials for enhanced removal of mercury from aqueous solution. Environmental Science and Pollution Research, 2019, 26(9): 8709-8720. https://doi.org/10.1007/s11356-019-04320-0

[42] Huang Y, Xia S, Lyu J, et al. Highly efficient removal of aqueous Hg^{2+} and CH_3Hg^+ by selective modification of biochar with 3-mercaptopropyltrimethoxysilane. Chemical Engineering Journal, 2019, 360: 1646-1655. https://doi.org/10.1016/j.cej.2018.10.231

[43] Liang X F, Xu Y M, Sun G H, et al. Preparation and characterization of mercapto functionalized sepiolite and their application for sorption of lead and cadmium. Chemical

Engineering Journal, 2011, 174(1): 436-444. https://doi.org/10.1016/j.cej.2011.08.060

[44] Mohan D, Singh P, Sarswat A, et al. Lead sorptive removal using magnetic and nonmagnetic fast pyrolysis energy cane biochars. Journal of Colloid and Interface Science, 2015, 448: 238-250. http://dx.doi.org/10.1016/j.jcis.2014.12.030

[45] China's Ministry of Environmental Protection. Chinese environmental quality standard for soils (GB 15618-2018). China's Ministry of Environmental Protection, 2018. http://kjs.mee.gov.cn/hjbhbz/bzwb/trhj/trhjzlbz/201807/t20180703_446029.shtml.

[46] Lindsay W L, Norvell W A. Development of a DTPA soil test for zinc, iron, manganese, and copper 1. Soil Science Society of America Journal, 1978, 42(3): 421-428. https://doi.org/10.2136/sssaj1978.03615995004200030009x

[47] Dai J. Heavy metal accumulation by two earthworm species and its relationship to total and DTPA-extractable metals in soils. Soil Biology and Biochemistry, 2004, 36(1): 91-98. https://doi.org/10.1016/j.soilbio.2003.09.001

[48] Tessier A, Campbell P G, Bisson M. Sequential extraction procedure for the speciation of particulate trace metals. Analytical Chemistry, 1979, 51(7): 844-851. https://doi.org/10.1021/ac50043a017

[49] Yakout S M. Monitoring the changes of chemical properties of rice straw–derived biochars modified by different oxidizing agents and their adsorptive performance for organics. Bioremediation Journal, 2015, 19(2): 171-182. https://doi.org/10.1080/10889868.2015.1029115

[50] Mahlangu T, Das R, Abia L K, et al. Thiol-modified magnetic polypyrrole nanocomposite: An effective adsorbent for the adsorption of silver ions from aqueous solution and subsequent water disinfection by silver-laden nanocomposite. Chemical Engineering Journal, 2019, 360: 423-434. https://doi.org/10.1016/j.cej.2018.11.231

[51] Bagheri S, Amini M M, Behbahani M, et al. Low cost thiol-functionalized mesoporous silica, KIT-6-SH, as a useful adsorbent for cadmium ions removal: a study on the adsorption isotherms and kinetics of KIT-6-SH. Microchemical Journal, 2019, 145: 460-

469. https://doi.org/10.1016/j.microc.2018.11.006

[52] Tsai W T, Liu S C, Chen H R, et al. Textural and chemical properties of swine-manure-derived biochar pertinent to its potential use as a soil amendment. Chemosphere, 2012, 89(2): 198-203. https://doi.org/10.1016/j.chemosphere.2012.05.085

[53] Wang P, Yin Y, Guo Y, et al. Removal of chlorpyrifos from waste water by wheat straw-derived biochar synthesized through oxygen-limited method. RSC Advances, 2015, 5(89): 72572-72578. https://doi.org/10.1039/c5ra10487d

[54] Mandal A, Singh N, Purakayastha T J. Characterization of pesticide sorption behaviour of slow pyrolysis biochars as low cost adsorbent for atrazine and imidacloprid removal. Science of the Total Environment, 2017, 577: 376-385. http://dx.doi.org/10.1016/j.scitotenv.2016.10.204

[55] Liang S, Guo X, Feng N, et al. Adsorption of Cu^{2+} and Cd^{2+} from aqueous solution by mercapto-acetic acid modified orange peel. Colloids and Surfaces B: Biointerfaces, 2009, 73(1): 10-14. https://doi.org/10.1016/j.colsurfb.2009.04.021

[56] Purakayastha T J, Kumari S, Pathak H. Characterisation, stability, and microbial effects of four biochars produced from crop residues. Geoderma, 2015, 239-240: 293-303. http://dx.doi.org/10.1016/j.geoderma.2014.11.009

[57] Li B, Yang L, Wang C Q, et al. Adsorption of Cd(II) from aqueous solutions by rape straw biochar derived from different modification processes. Chemosphere, 2017, 175: 332-340. http://dx.doi.org/10.1016/j.chemosphere.2017.02.061

[58] Ozgenc O, Durmaz S, Boyaci I H, et al. Determination of chemical changes in heat-treated wood using ATR-FTIR and FT Raman spectrometry. Spectrochimica Acta. Part A: Molecular and Biomolecular Spectroscopy, 2017, 171: 395-400. http://dx.doi.org/10.1016/j.saa.2016.08.026

[59] Sun J, Gu X, Dong Q, et al. Durable flame-retardant finishing for polyamide 66 fabrics by surface hydroxymethylation and crosslinking. Polymers for Advanced Technologies,

2013, 24(1): 10-14. https://doi.org/10.1002/pat.3041

[60] Zhang X H, Wang S F. Voltametric behavior of noradrenaline at 2-mercaptoethanol self-assembled monolayer modified gold electrode and its analytical application. Sensors, 2003, 3(3): 61-68. https://doi.org/10.3390/s30300061

[61] Matuana L M, Balatinecz J J, Sodhi R N S, et al. Surface characterization of esterified cellulosic fibers by XPS and FTIR spectroscopy. Wood Science and Technology, 2001, 35(3): 191-201. https://doi.org/10.1007/s002260100097

[62] Pham C V, Eck M, Krueger M. Thiol functionalized reduced graphene oxide as a base material for novel graphene-nanoparticle hybrid composites. Chemical Engineering Journal, 2013, 231: 146-154. http://dx.doi.org/10.1016/j.cej.2013.07.007

[63] Aldana-Pérez A, Lartundo-Rojas L, Gómez R, et al. Sulfonic groups anchored on mesoporous carbon Starbons-300 and its use for the esterification of oleic acid. Fuel, 2012, 100: 128-138. https://doi.org/10.1016/j.fuel.2012.02.025

[64] Desroches M, Caillol S, Auvergne R, et al. Biobased cross-linked polyurethanes obtained from ester/amide pseudo-diols of fatty acid derivatives synthesized by thiol–ene coupling. Polym. Chem., 2012, 3(2): 450-457. http:// doi.org/10.1039/c1py00479d

[65] Tan G, Sun W, Xu Y, et al. Sorption of mercury (II) and atrazine by biochar, modified biochars and biochar based activated carbon in aqueous solution. Bioresource Technology, 2016, 211: 727-735. http://dx.doi.org/10.1016/j.biortech.2016.03.147

[66] Febrianto J, Kosasih A N, Sunarso J, et al. Equilibrium and kinetic studies in adsorption of heavy metals using biosorbent: a summary of recent studies. Journal of Hazardous Materials, 2009, 162(2-3): 616-645. https://doi.org/10.1016/j.jhazmat.2008.06.042

[67]Sun Q, Aguila B, Perman J, et al. Postsynthetically modified covalent organic frameworks for efficient and effective mercury removal. Journal of the American Chemical Society, 2017, 139(7): 2786-2793. https://doi.org/10.1021/jacs.6b12885

[68]Zhang F, Wang X, Yin D, et al. Efficiency and mechanisms of Cd removal from aqueous solution by biochar derived from water hyacinth (*Eichornia crassipes*). Journal of

Environmental Management, 2015, 153: 68-73. https://doi.org/10.1016/j.jenvman.2015.01.043

[69]Srinivasan P, Sarmah A K, Smernik R, et al. A feasibility study of agricultural and sewage biomass as biochar, bioenergy and biocomposite feedstock: production, characterization and potential applications. Science of the Total Environment, 2015, 512: 495-505. https://doi.org/10.1016/j.scitotenv.2015.01.068

[70] Niu Q, Luo J, Xia Y, et al. Surface modification of bio-char by dielectric barrier discharge plasma for Hg^0 removal. Fuel Processing Technology, 2017, 156: 310-316. https://doi.org/10.1016/j.fuproc.2016.09.013

[71] Pearson R G. Hard and soft acids and bases. Journal of the American Chemical society, 1963, 85(22), 3533-3539. https://doi.org/10.1021/ja00905a001

[72] Park J H, Ok Y S, Kim S H, et al. Competitive adsorption of heavy metals onto sesame straw biochar in aqueous solutions. Chemosphere, 2016, 142: 77-83. http://dx.doi.org/10.1016/j.chemosphere.2015.05.093

[73] Deng S, Wang P, Zhang G, et al. Polyacrylonitrile-based fiber modified with thiosemicarbazide by microwave irradiation and its adsorption behavior for Cd (II) and Pb (II). Journal of hazardous materials, 2016, 307, 64-72. https://doi.org/10.1016/j.jhazmat.2016.01.002

[74] Pehlivan E, Yanik B H, Ahmetli G, et al. Equilibrium isotherm studies for the uptake of cadmium and lead ions onto sugar beet pulp. Bioresource Technology, 2008, 99(9): 3520-3527. https://doi.org/10.1016/j.biortech.2007.07.052

[75] Tan X, Liu Y, Zeng G, et al. Application of biochar for the removal of pollutants from aqueous solutions. Chemosphere, 2015, 125: 70-85. http://dx.doi.org/10.1016/j.chemosphere.2014.12.058

[76] Fan L, Zhou A, Zhong L, et al. Selective and effective adsorption of Hg (II) from aqueous solution over wide pH range by thiol functionalized magnetic carbon nanotubes.

Chemosphere, 2019, 226: 405-412. https://doi.org/10.1016/j.chemosphere.2019.03.154

[77] Liu Z, Ling X Y, Guo B, et al. Pt and PtRu nanoparticles deposited on single-wall carbon nanotubes for methanol electro-oxidation. Journal of Power Sources, 2007, 167(2): 272-280. https://doi.org/10.1016/j.jpowsour.2007.02.044

[78] Huang Y, Gong Y, Tang J, et al. Effective removal of inorganic mercury and methylmercury from aqueous solution using novel thiol-functionalized graphene oxide/Fe-Mn composite. Journal of hazardous materials, 2019, 366: 130-139. https://doi.org/10.1016/j.jhazmat.2018.11.074

[79] Huang Q, Chen Y, Yu H, et al. Magnetic graphene oxide/MgAl-layered double hydroxide nanocomposite: One-pot solvothermal synthesis, adsorption performance and mechanisms for Pb^{2+}, Cd^{2+}, and Cu^{2+}. Chemical Engineering Journal, 2018, 341: 1-9. https://doi.org/10.1016/j.cej.2018.01.156

[80] Wu A, Tian C, Jiao Y, et al. Sequential two-step hydrothermal growth of MoS_2 /CdS core-shell heterojunctions for efficient visible light-driven photocatalytic H_2 evolution. Applied Catalysis B: Environmental, 2017, 203: 955-963. http://dx.doi.org/10.1016/j.apcatb.2016.11.009

[81] Sharma A S, Biswas K, Basu B. Fine scale characterization of surface/subsurface and nanosized debris particles on worn Cu–10 % Pb nanocomposites. Journal of Nanoparticle Research, 2013, 15(5): 1675. https://doi.org/10.1007/s11051-013-1675-5

[82] Zheng X, Lei H, Yang G, et al. Enhancing efficiency and stability of perovskite solar cells via a high mobility p-type PbS buffer layer. Nano Energy, 2017, 38: 1-11. https://doi.org/10.1016/j.nanoen.2017.05.040

[83] Wang L, Shi Y, Yao D, et al. Cd complexation with mercapto-functionalized attapulgite (MATP): adsorption and DFT study. Chemical Engineering Journal, 2019, 366: 569-576. https://doi.org/10.1016/j.cej.2019.02.114

[84] Houben D, Evrard L, Sonnet P. Beneficial effects of biochar application to contaminated soils on the bioavailability of Cd, Pb and Zn and the biomass production of rapeseed

(*Brassica napus* L.). Biomass & Bioenergy, 2013, 57: 196-204. https://doi.org/10.1016/j.biombioe.2013.07.019

[85] Lei O, Zhang R D. Effects of biochars derived from different feedstocks and pyrolysis temperatures on soil physical and hydraulic properties. Journal of Soils and Sediments, 2013, 13(9): 1561-1572. https://doi.org/10.1007/s11368-013-0738-7

[86] Cheng C H, Lehmann J, Engelhard M H. Natural oxidation of black carbon in soils: Changes in molecular form and surface charge along a climosequence. Geochimica et Cosmochimica Acta, 2008, 72(6): 1598-1610. https://doi.org/10.1016/j.gca.2008.01.010

[87] Lucchini P, Quilliam R S, Deluca T H, et al. Does biochar application alter heavy metal dynamics in agricultural soil?. Agriculture, Ecosystems & Environment, 2014, 184: 149-157. https://doi.org/10.1016/j.agee.2013.11.018

[88] He L, Li N, Liang X, et al. Reduction of Cd accumulation in pak choi (*Brassica chinensis* L.) in consecutive growing seasons using mercapto-grafted palygorskite. RSC Advances, 2018, 8(56): 32084-32094. https://doi.org/10.1039/C8RA04952A

[89] Lian M, Feng Q, Wang L, et al. Highly effective immobilization of Pb and Cd in severely contaminated soils by environment-compatible, mercapto-functionalized reactive nanosilica. Journal of Cleaner Production, 2019, 235: 583-589. https://doi.org/10.1016/j.jclepro.2019.07.015

[90] Liang X F, Han J, Xu Y M, et al. *In situ* field-scale remediation of Cd polluted paddy soil using sepiolite and palygorskite. Geoderma, 2014, 235: 9-18. https://doi.org/10.1016/j.geoderma.2014.06.029

[91] Li X, Peng W, Jia Y, et al. Bioremediation of lead contaminated soil with *Rhodobacter sphaeroides*. Chemosphere, 2016, 156: 228-235. https://doi.org/10.1016/j.chemosphere.2016.04.098

[92] Yang X, Lu K, Mcgrouther K, et al. Bioavailability of Cd and Zn in soils treated with biochars derived from tobacco stalk and dead pigs. Journal of Soils and Sediments, 2017,

17(3): 751-762. https://doi.org/10.1007/s11368-015-1326-9

[93] Park J H, Choppala G K, Bolan N S, et al. Biochar reduces the bioavailability and phytotoxicity of heavy metals. Plant and Soil, 2011, 348(1-2): 439-451. https://doi.org/10.1007/s11104-011-0948-y

[94] Galvez-Cloutier R, Dubé J-S. An evaluation of fresh water sediments contamination: the Lachine Canal sediments case, Montréal, Canade. Part II: heavy metal particulate speciation study. Water, Air, and Soil Pollution, 1998, 102(3-4): 281-302. https://doi.org/10.1023/A:1004900624880

Figure caption

Fig. 1 FT-IR spectra of RB and RS.

Fig. 2 Overview of the RS preparation

Fig. 3 Sorption kinetic of (a) Cd^{2+} and (b) Pb^{2+} onto RB and RS (initial concentration of metal ions: 200 mg L^{-1}, adsorbent dosage: 2.5 g L^{-1}, pH 5, buffered by 0.05 mol L^{-1} acetic acid).

Fig. 4 Sorption isotherms of (a) Cd^{2+} and (b) Pb^{2+} on RB and RS in the single-metal systems (adsorbent dosage: 2.5 g L^{-1}, pH 5, buffered by 0.05 mol L^{-1} acetic acid).

Fig. 5 Sorption isotherms of Cd^{2+} and Pb^{2+} on RB and RS in the binary-metal systems (adsorbent dosage: 2.5 g L^{-1}, pH 5, buffered by 0.05 mol L^{-1} acetic acid, contact time: 24 h).

Fig. 6 XPS spectra of (a) S2p for RS before and after cadmium and lead uptake, (b) Cd3d for RB-Cd^{2+}, (c) Cd3d for RS-Cd^{2+}, (d) Pb4f for RB-Pb^{2+} and (e) Pb4f for RS-Pb^{2+}.

Fig. 7 Effect of RB and RS on availability of (a) Cd and (b) Pb. Different lower case and capital letters above the column indicate significant difference between treatments at $p < 0.05$.

Fig. 8 Influence of RB and RS on species distribution of (a) Cd and (b) Pb.

Table 1 Soil properties

pH	CEC (cmol kg^{-1})	O.M. (%)	Clay (%)	Silt (%)	Sand (%)	Cd (mg kg^{-1})	Pb (mg kg^{-1})
7.42	13.53	2.15	0.76	18.74	80.50	9.18	1182

Table 2 Physicochemical properties of RB and RS.

	CNS elements			-SH content (mmol g^{-1})	pH	pH_{PZC}	surface area (m^2 g^{-1})	pore diameter (nm)
	N (%)	C (%)	S (%)					
RB	1.54	48.18	0.98	0.01	10.20	9.92	7.82	20.82
RS	0.59	43.71	24.04	0.83	2.36	2.26	0.34	16.69

Table 3 Sorption kinetic parameters of Cd^{2+} and Pb^{2+} sorption on RB and RS (initial concentration of metal ions: 200 mg L^{-1}, adsorbent dosage: 2.5 g L^{-1}, pH 5, buffered by 0.05 mol L^{-1} acetic acid)

Ions	Sorbent	1st order kinetics			2nd order kinetics		
		q_{m1} (mg g^{-1})	k_1 (h^{-1})	R^2	q_{m2} (mg g^{-1})	k_2 (g mg^{-1} h^{-1})	R^2
Cd^{2+}	RB	9.9	0.15	0.9963	11.3	0.01	0.9074
Cd^{2+}	RS	45.2	14.49	0.7221	46.1	0.60	0.9993
Pb^{2+}	RB	55.4	32.60	0.0246	55.6	1.90	0.9998
Pb^{2+}	RS	53.2	22.93	0.9750	54.3	1.13	0.9998

Table 4 Isotherm parameters of Langmuir and Freundlich for the sorption of Cd^{2+} and Pb^{2+} onto RB and RS in the single-metal systems (adsorbent dosage: 2.5 g L^{-1}, pH 5, buffered by 0.05 mol L^{-1} acetic acid, contact time 24 h)

Isotherm	Parameters	Cd^{2+}	Cd^{2+}	Pb^{2+}	Pb^{2+}
		RB	RS	RB	RS
Langmuir	Q_m (mg g^{-1})	14.2	45.1	67.4	61.4
	K_L (L mg^{-1})	0.01	0.22	0.09	0.03
	R^2	0.8143	0.9993	0.9965	0.9982
Freundlich	K_F (mg g^{-1})	1.8	24.0	20.3	9.5
	1/n	0.31	0.12	0.25	0.31
	R^2	0.4154	0.9899	0.9168	0.9248

Table 5 Isotherm parameters of Langmuir and Freundlich for the sorption of Cd^{2+} and Pb^{2+} onto RB and RS in the binary-metal systems (adsorbent dosage: 2.5 g L^{-1}, pH 5, buffered by 0.05 mol L^{-1} acetic acid, contact time: 24 h)

Isotherm	Parameters	RB		RS	
		Cd^{2+}	Pb^{2+}	Cd^{2+}	Pb^{2+}
Langmuir	Q_m (mg g^{-1})	6.8	63.3	40.4	30.0
	K_L (L mg^{-1})	0.02	0.14	0.22	0.03
	R^2	0.8410	0.9854	0.9956	0.9824
Freundlich	K_F (mg g^{-1})	0.5	20.5	19.0	5.2
	1/n	0.44	0.17	0.14	0.29
	R^2	0.4314	0.4102	0.8272	0.9763

Table 6 Distribution and selectivity coefficient of competitive adsorption

	$K_{d\,(Cd)}$	$K_{d\,(Pb)}$	$K_{d\,(Cd)} / K_{d\,(Pb)}$	$K_{d\,(Pb)} / K_{d\,(Cd)}$
RB	14.39	119.59	0.12	8.31
RS	90.66	52.35	1.73	0.58

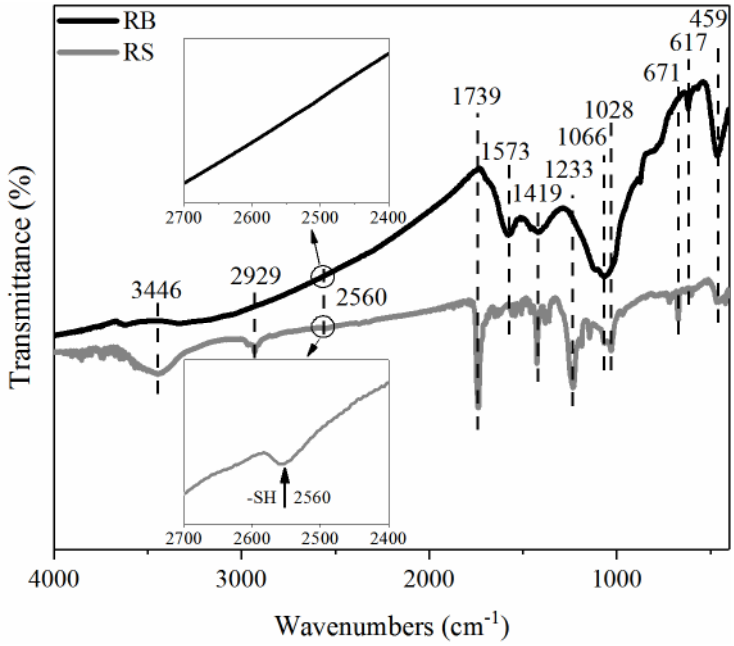
RB
RS
459
617
671
1739
1028
1066
1573
1233
1419
3446
2929
2560
-SH
2560
2700
2600
2500
2400
4000
3000
2000
1000
Transmittance (%)
Wavenumbers (cm-1)

Fig. 1

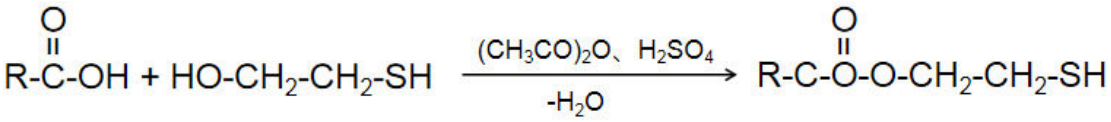

Fig. 2

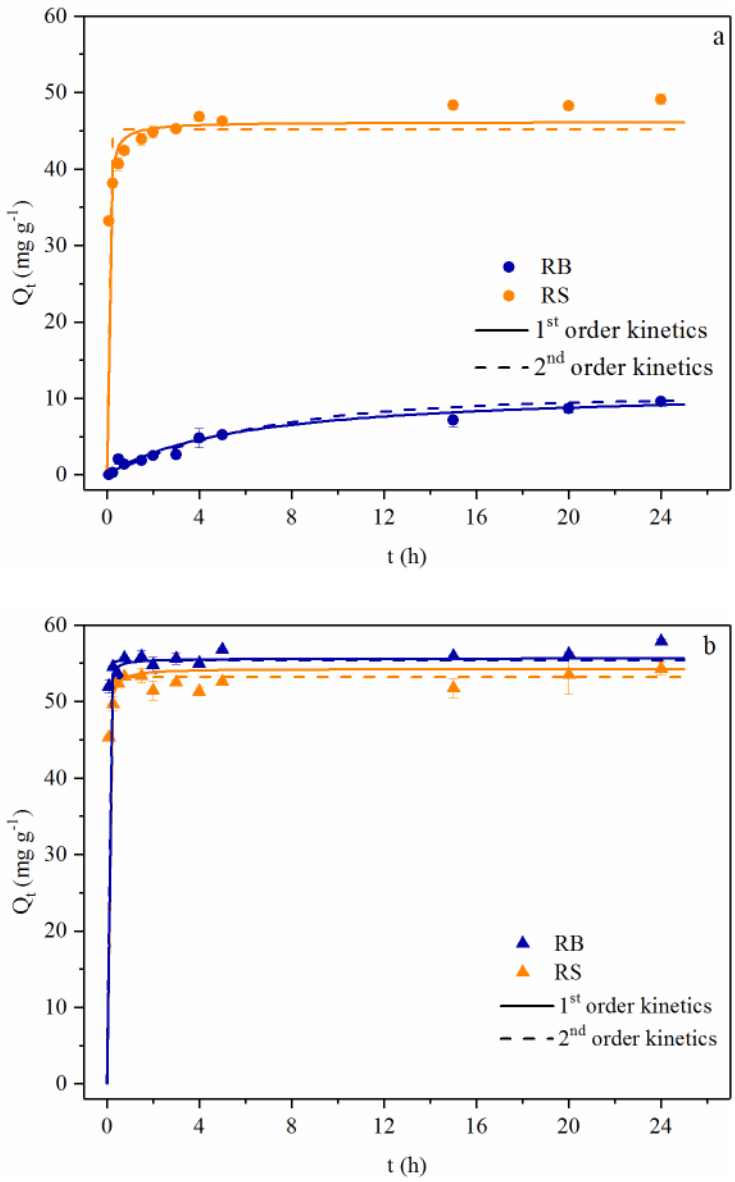
a
Q_t (mg g^{-1})
t (h)
RB
RS
1st order kinetics
2nd order kinetics
b
Q_t (mg g^{-1})
t (h)
RB
RS
1st order kinetics
2nd order kinetics

Fig. 3

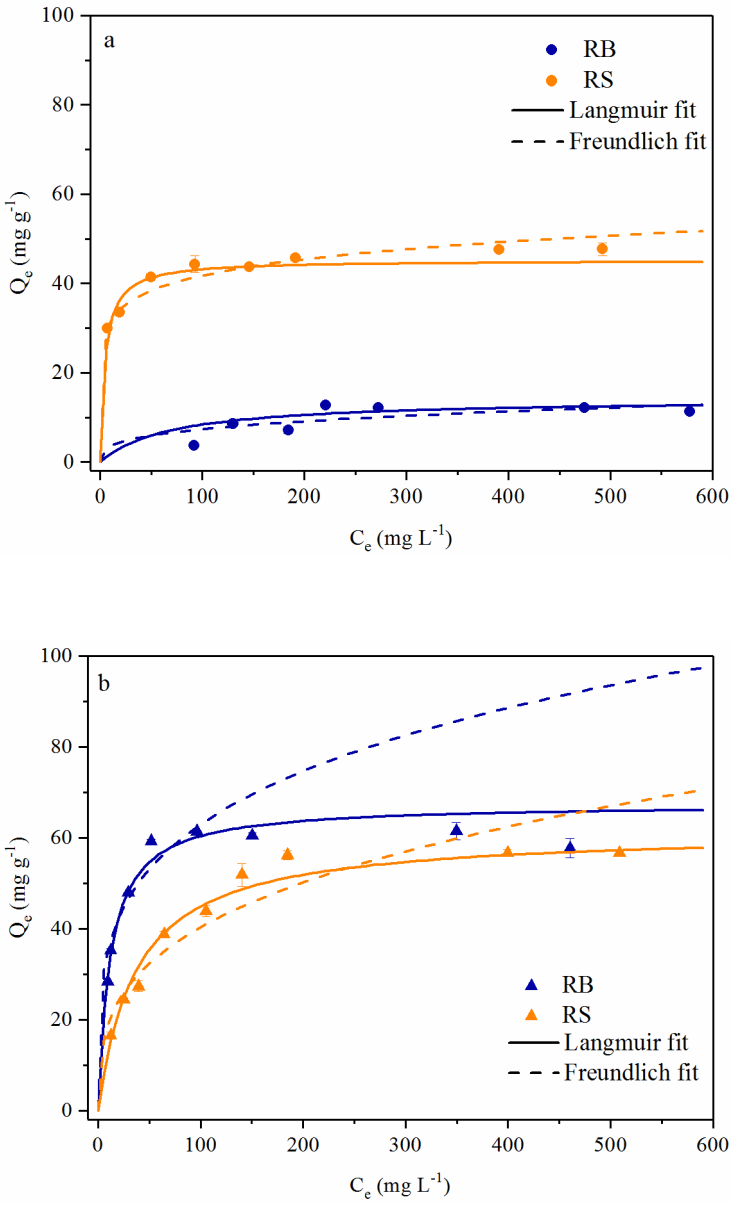
a
RB
RS
Langmuir fit
Freundlich fit
Q_e (mg g^{-1})
C_e (mg L^{-1})
b
RB
RS
Langmuir fit
Freundlich fit
Q_e (mg g^{-1})
C_e (mg L^{-1})

Fig. 4

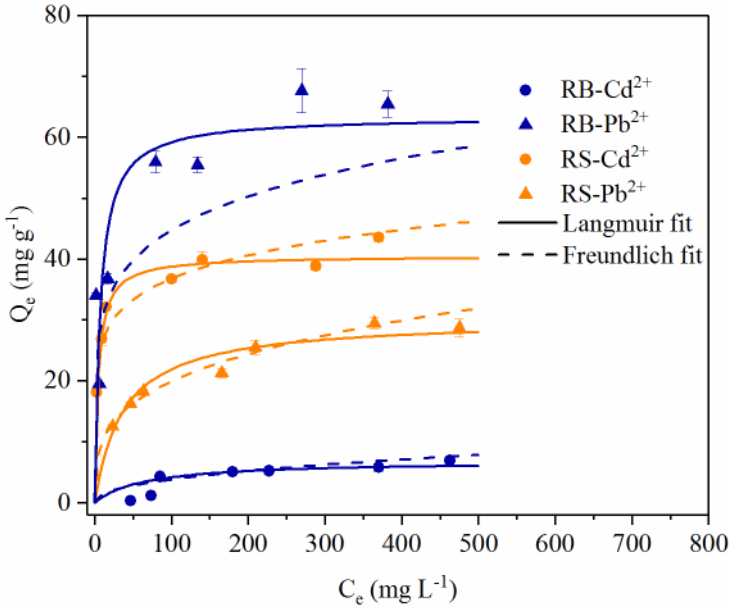
80
60
40
20
0
0
100
200
300
400
500
600
700
800
Q_e (mg g^{-1})
C_e (mg L^{-1})
RB-Cd^{2+}
RB-Pb^{2+}
RS-Cd^{2+}
RS-Pb^{2+}
Langmuir fit
Freundlich fit

Fig. 5

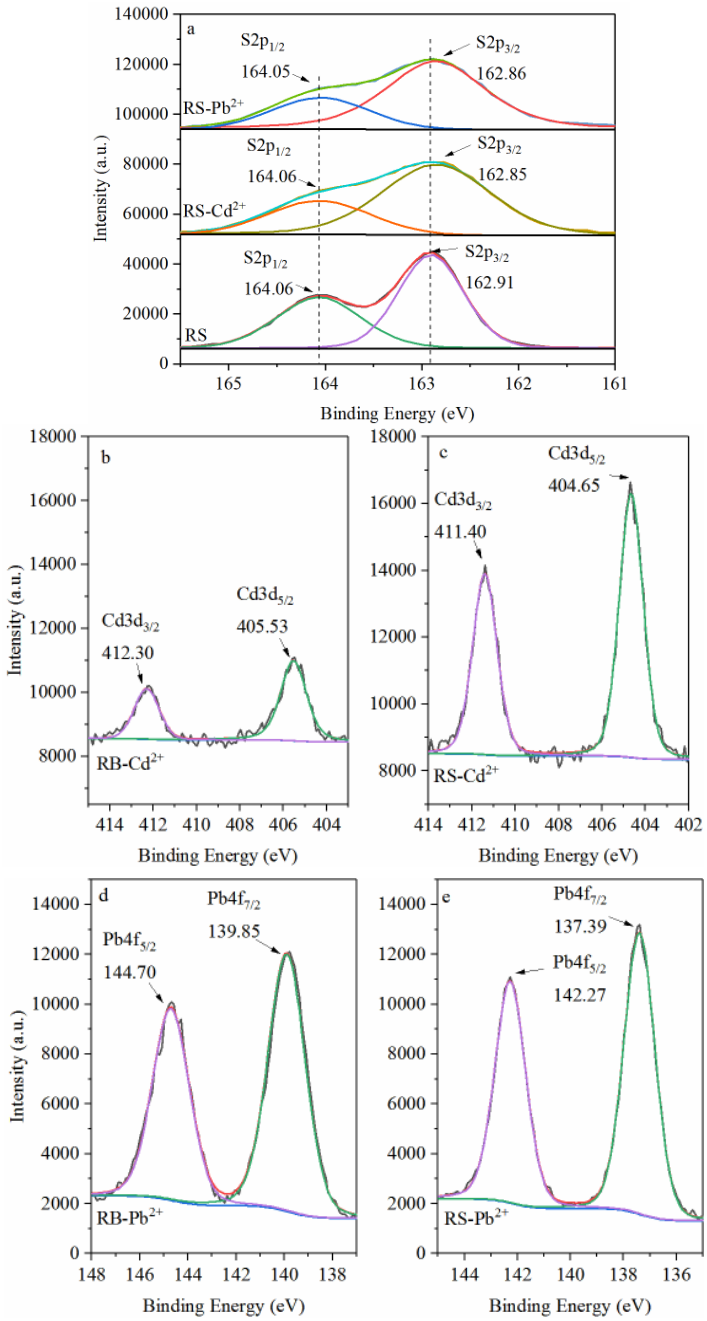
a
S2p1/2
164.05
S2p3/2
162.86
RS-Pb2+
S2p1/2
164.06
S2p3/2
162.85
RS-Cd2+
S2p1/2
164.06
S2p3/2
162.91
RS
Intensity (a.u.)
Binding Energy (eV)
b
Cd3d3/2
412.30
Cd3d5/2
405.53
RB-Cd2+
c
Cd3d5/2
404.65
Cd3d3/2
411.40
RS-Cd2+
d
Pb4f7/2
139.85
Pb4f5/2
144.70
RB-Pb2+
e
Pb4f7/2
137.39
Pb4f5/2
142.27
RS-Pb2+

Fig. 6

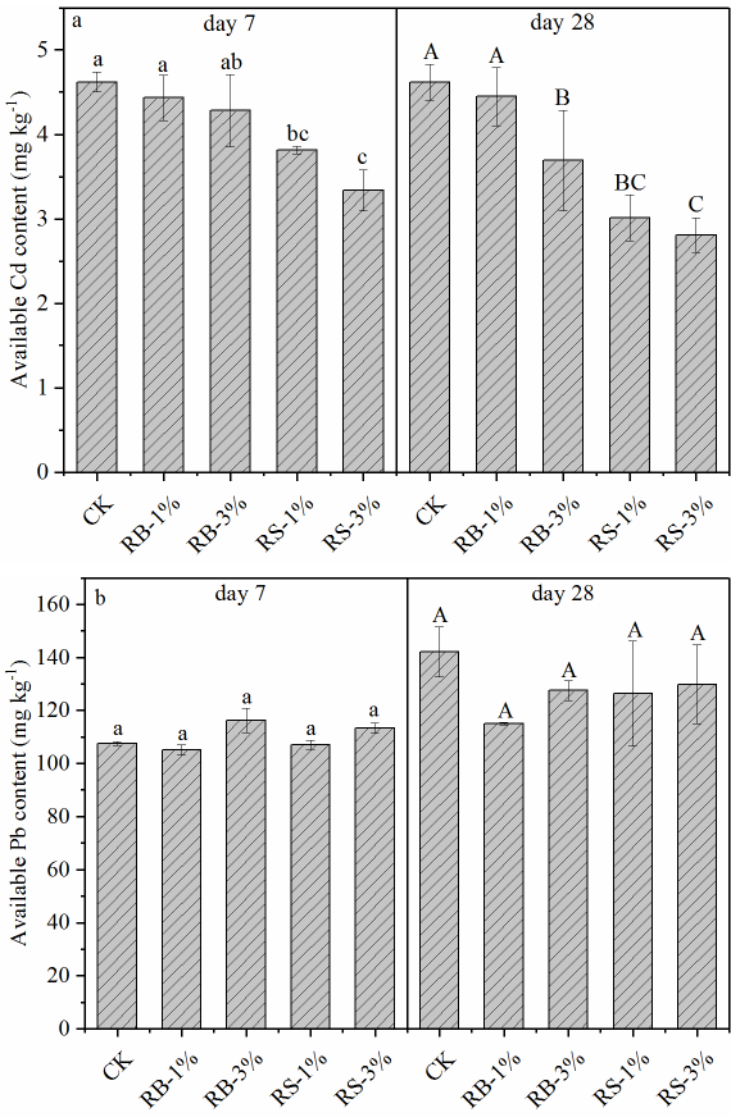
a
day 7
day 28
Available Cd content (mg kg-1)
a
a
ab
bc
c
A
A
B
BC
C
CK
RB-1%
RB-3%
RS-1%
RS-3%
b
day 7
day 28
Available Pb content (mg kg-1)
a
a
a
a
a
A
A
A
A
A

Fig. 7

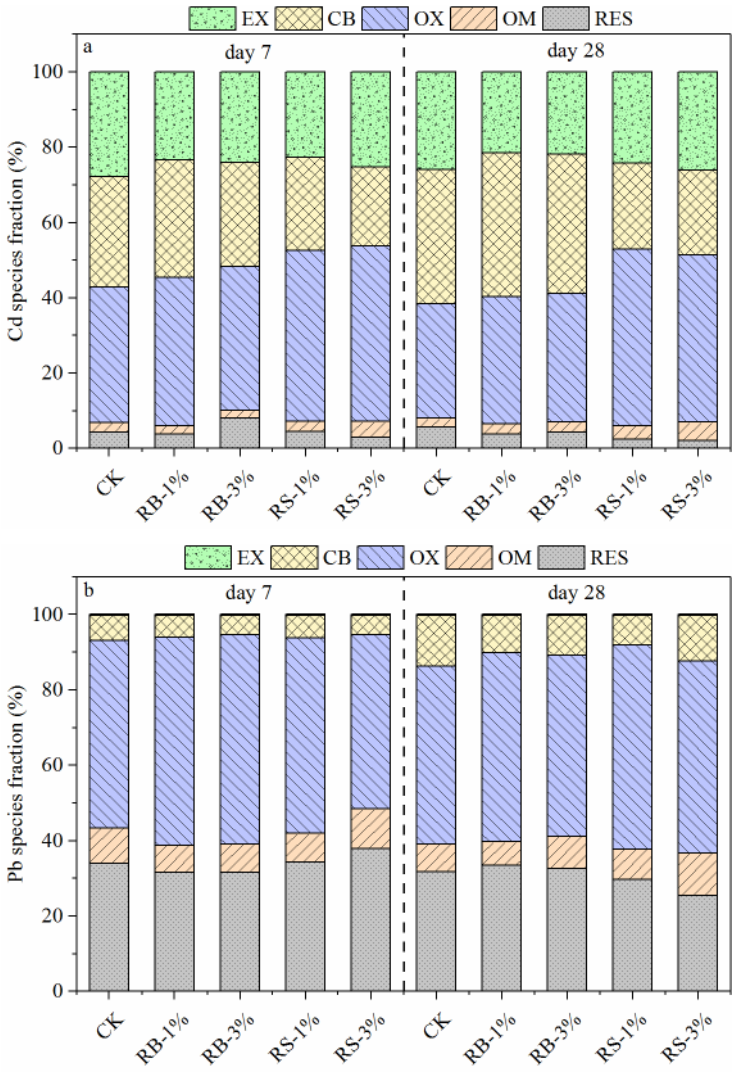
EX
CB
OX
OM
RES
a
day 7
day 28
Cd species fraction (%)
0
20
40
60
80
100
CK
RB-1%
RB-3%
RS-1%
RS-3%
CK
RB-1%
RB-3%
RS-1%
RS-3%
EX
CB
OX
OM
RES
b
day 7
day 28
Pb species fraction (%)
0
20
40
60
80
100
CK
RB-1%
RB-3%
RS-1%
RS-3%
CK
RB-1%
RB-3%
RS-1%
RS-3%

Fig. 8